59th ILMENAU SCIENTIFIC COLLOQUIUM
Technische Universität Ilmenau, 11 – 15 September 2017
URN: urn:nbn:de:gbv:ilm1-2017iwk-079:2

Pattern sequences for fast absolute phase retrieval with application in the handheld operation of structured light sensors

Steffen Matthias, Markus Kästner, Eduard Reithmeier

Institute of Measurement and Automatic Control, Leibniz Universität Hannover,
Nienburger Str. 17, 3067 Hannover

ABSTRACT

Areal 3D scanners based on structured light projection are widely used for inspection tasks in manufacturing processes. For accurate measurements of object geometries, common structured light sensors project a sequence of periodic patterns onto the surface. By subsequent evaluation of these patterns, the local phase of the patterns is reconstructed in a phase retrieval step. The local phase encodes the geometry information and allows for the reconstruction of 3D point clouds in combination with a calibration of the sensor. However, motion of an object during the projection of the pattern sequence leads to large deviations in the reconstructed local phase and thus the 3D point cloud. For dynamic measurements of moving objects, several single-shot techniques have been proposed. While these techniques only require a single pattern for 3D measurements, phase reconstruction suffers when measuring non-diffuse reflective surfaces. In order to evaluate the feasibility of different approaches, sequences of periodic patterns with different lengths are compared based on static and dynamic measurements of a contour standard with a non-diffuse surface using a fiber-endoscopic structured light sensor. Based on the evaluations, pattern sequences are parametrized for dynamic measurements using the flexible sensor head of the endoscopic system. A proof of concept of simultaneous localization and mapping for the handheld operation of the endoscopic sensor head is demonstrated, which can be used for the navigation in narrow spaces in the future.

Index Terms **–** Endoscopy, Motion, Localization, 3D reconstruction, Tracking

1. INTRODUCTION

Optical inspection techniques are widely used as an alternative to tactile methods in manufacturing processes [1]. The combination of their non-destructive nature with high measuring speeds for complete surface areas enable their use in the production line. Structured light sensors are capable of measuring surface areas with diameters up to a few meters in less than ten seconds. There are however still a number of challenges which prevent the use of these sensors for certain inspection applications. Size and speed of the measuring devices are critical for inline measurements. Other limiting factors are surface texture and reflectivity, which can introduce noise and uncovered areas in measurements. Relative motion between sensor and specimen leads to undesired deviations in the acquired data or invalid measurements. Motion is present when an object is for example moving on a transportation belt in the production line, but also due to vibrations arising from production machines in proximity to the measuring position. Recent progresses in structured illumination devices and cameras allow for shorter acquisition times and higher framerates, enabling the use of structured light projectors for the measurement of dynamic scenes. For this purpose, specifically adapted pattern single-pattern approaches and short pattern sequences have been

proposed. In general, these techniques need to make a trade-off between measuring speed, robustness towards surface reflectivity and texture, constraints on the geometry of the object, or constraints on the design of the measuring device. Followed by a discussion of state-of-the-art pattern encoding techniques, a new coding scheme is proposed in this paper. The proposed periodic interleaved pattern sequence allows for high 3-D imaging rates, while being robust towards varying surface reflectivity to avoid the need to apply diffuse reflective spray on the measuring object. Furthermore, an approach for the registration and merging of point clouds, based on a weighted iterative closest point algorithm, is presented. Individual measurements of a measured 3-D sequence are registered into a common coordinate system, enabling both measurements of large surface areas and tracking of the sensor's position. The feasibility of the implemented approaches in practical situations is demonstrated by measurements with an endoscopic structured light sensor, which has been developed for the in-situ inspection of metal forming processes [2]. Next to evaluations of reference objects in motion, hand guided measurement is shown, which has potential for the localization of the sensor head in enclosed spaces, for example in machine inspection. Potential applications of the sensor include in-situ measurements in forming machines or the inspection of hard-to-access machine parts. For performing in-situ inspections, a short measurement time is desired to reduce influences of vibrations and meet the required cycle time. Inspection tasks in enclosed spaces would additionally benefit from the capability to localize the sensor head based on continuously measured 3-D data.

2. CODED PATTERN SEQUENCES

Structured light scanning, also called active stereo or fringe projection profilometry, is a 3-D measuring technique based on triangulation and coded light patterns. A structured light sensor typically consists of one projector and one or two cameras; however designs with more than one projector or more than two cameras are used in some applications. In order to triangulate 3-D point clouds of a surface, per-pixel correspondences between camera and projector need to be found. This is achieved by projecting a coded pattern and observation of the deformed pattern in the camera images. By decoding the patterns on the camera side, correspondences to the projector for subsequent triangulation are found. As a result, next to accurate calibration of the geometrical setup of the sensor, the pattern coding strategy is critical for the achievable measurement uncertainty. Coding strategies depending on the projection of several patterns usually achieve lower noise than short sequences or single pattern approaches. However, when relative motion between specimen and sensor is present, multi-pattern sequences suffer from motion artifacts due to the longer acquisition time required.
Most pattern encoding strategies can be categorized into the following groups:

- Binary code patterns [3],
- Sinusoidal patterns [4],
- Line/Grid patterns [5],
- Stochastic patterns [6].

In order to achieve unambiguous correspondences, these codification strategies generally modulate the projected light intensity in time and/or spatially. In addition to intensity, color can be modulated; this however requires a capable projector and optically cooperative specimen. For measurements of non-moving specimen, sequences of sinusoidal patterns are commonly used, owing to their capability of obtaining correspondences with sub-pixel accuracy in combination with temporal phase-unwrapping [7]. For single-shot patterns based on sinusoidal patterns, several frequencies are combined into a single pattern by multiplication or color coding [8,9]. Generally, sinusoidal based single-shot patterns suffer

from phase distortions when measuring objects with highly varying texture and reflectivity, such as technical surfaces, as will be discussed further in Section 3.
In [10], a three step phase-shift is used, which can compensate the influence of the surface, in combination geometrical constraint based phase unwrapping. This approach however requires at least two cameras for the unwrapping process.
Single-image line or grid patterns are robust to surface texture by using locally adaptive thresholds for example. However they allow for the calculation of 3D points at the line positions, resulting in less dense point clouds than other approaches. Additionally, the line detection is less robust to defocus than sinusoidal patterns, as the line contrast significantly decreases in case of slight defocus.

3. INTERLEAVED MULTI-FREQUENCY SEQUENCE

Phase recovery is performed similar to the approach introduced by Takeda [11]. However, instead of a single pattern, three patterns are used. The technique introduced in [11] has two main limitations; firstly, technical surfaces with highly varying reflectivity cannot be measured, secondly, the geometry of the specimen is assumed to be continuous to allows for spatial phase unwrapping. The two limitations are overcome by adding two additional patterns, at the cost of a higher acquisition time, in combination with an approximation for surface reflectivity in the phase evaluation algorithm. The three patterns required for absolute phase retrieval are furthermore extended to a periodic sequence, which enables phase recovery from any three adjacent images of the sequence by employing a symmetric design. As a result, a 3-D capture rate equal to the camera's image acquisition rate is achieved, which significantly reduces latency in the acquisition process when compared to other three-pattern algorithms.
In order to motivate the design of the patterns, first properties of phase-shift patterns in spatial and frequency domain are discussed. The intensity at a given pixel $g(x,y)$ of a phase shift sequence of length N can be expressed by Equation 1, where a is the background illumination component and b is the amplitude modulation component. The patterns are modulated in direction of x with a frequency of ω_c. The phase is locally modulated by $\Delta\varphi(x,y)$ owing to the geometry of the object, while the patterns with index $n = 0 \dots N-1$ are shifted equally over 2π.

$$g_n(x,y) = a(x,y) + b(x,y)\cos(\omega_c x + \Delta\varphi(x,y) + n\frac{2\pi}{N}) \tag{1}$$

If assuming for simplicity the case of $\Delta\varphi(x,y) = 0$, e.g. no deformation of the projected patterns, the Fourier transform for g_0 is shown in Equation 2.

$$F\{g_0(x,y)\} = A(i\Omega) + \frac{1}{2}B(i\Omega - \Omega_0) + \frac{1}{2}B(i\Omega + \Omega_0) \tag{2}$$

For diffuse reflective specimen, A and B exhibit low bandwidth, allowing for separation of the components and the recovery of the relative local phase by assuming low variation in B compared to the local modulation of the phase $\Delta\varphi$ [11]. However, if the specimen features varying texture and reflectivity, which is the case for almost all technical surfaces, spectral components of A and B overlap. The effect is illustrated in Figure 1 a), where 3 peaks are evident, arising from the constant and cosine components of the pattern. As discussed in Section 2, the components can be separated by choosing a pattern count of $N \geq 3$. For fewer

patterns, not all components can be separated if overlap is present. In this case, phase recovery without large distortions is not possible.
If $N = 2$ is chosen with a shift offset of π between the first and the added second pattern, the central background component can be estimated by $a = g_0 + g_1$ and therefore be removed from the center of the spectrum, as illustrated in Figure 1 b). While the two remaining cosine-components are further separated from each other than from the central component in the spectrum, there are still overlapping areas for objects with varying reflectivity, especially if lower pattern frequencies are chosen. To remove the overlap, which is caused by the reflectivity of the pattern, contribution factors of environment and sensor to *a* and/or *b* are considered:

- Vignetting (*a, b*),
- Defocus (*a, b*),
- Ambient light (*a*),
- Surface reflectivity and texture (*a, b*).

Under practical conditions, Surface reflectivity is the dominating influence on both *a* and *b*. Ambient light is typically not directed onto the surface and for most sensors significantly lower in intensity than the light emitted by the projector. Vignetting, which can occur due to depending on camera or projector optics, has similar effects on *a* and *b*, while defocus has more effect on *b* due the modulated illumination. However, their influence can be assumed to be small compared to the contribution of surface reflectivity and texture. Therefore, *a* is assumed to be a good approximation of surface reflectivity and texture. Dividing patterns in spatial domain by *a* is equal to the deconvolution of the reflectivity in frequency domain, resulting in narrowing of the peaks, as illustrated in Figure 1 c). As ideally no remaining overlap is present, one of the two components can be suppressed by employing a mask in the frequency domain. After applying the inverse Fourier transform to the bandpass filtered spectrum, an approximation of the analytic signal is obtained, which contains the local phase of the pattern. As long as influences of defocus and ambient light are kept small, the phase can accurately be recovered.

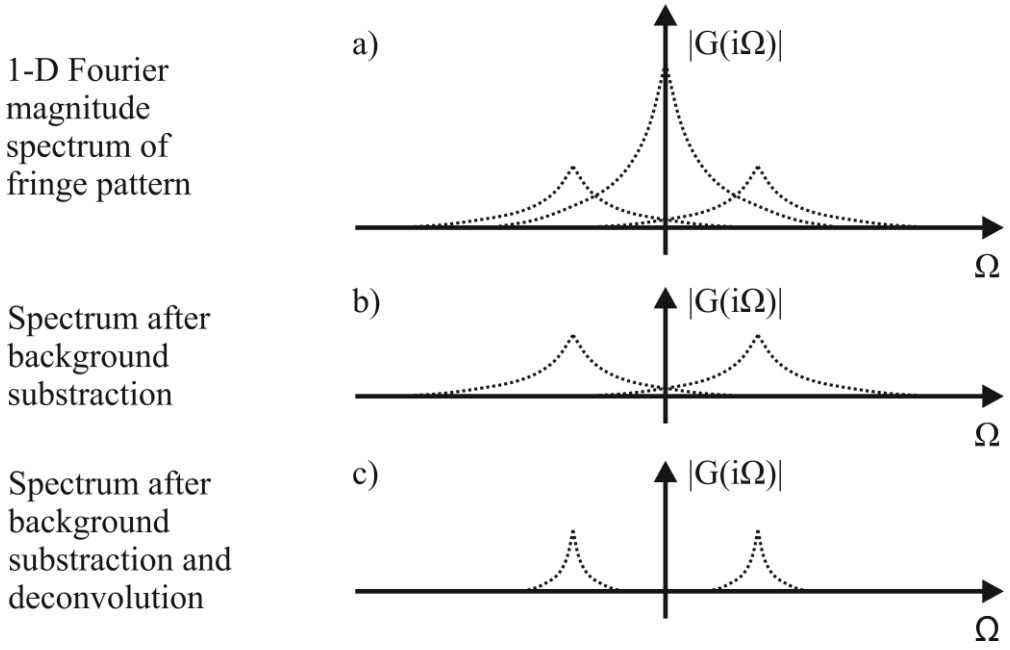

Figure 1: Fourier spectra of pattern images at different processing stages.

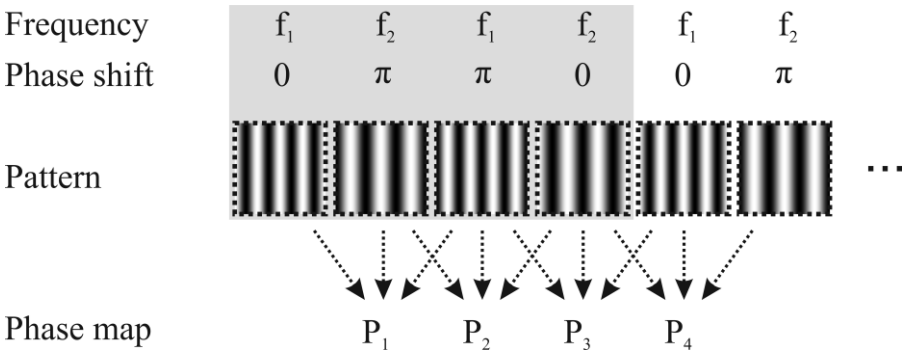

Figure 2: Interleaved pattern sequence.

The previous assumptions lead to the design of the proposed three-pattern algorithm. Two patterns of same frequency with a relative phase-shift of π are required to estimate the per-pixel surface reflectivity. A third pattern of a second frequency is added to allow for robust unwrapping of the absolute phase without requiring constraints on the object's surface or sensor design. Furthermore, the patterns are arranged to a periodic sequence with interleaved frequencies, in which any three neighboring patterns fulfill the requirements for the outlined three-pattern algorithm. Six patterns of the interleaved pattern sequence with an exemplary frequency are shown in Figure 2. The sequence has a period length of four patterns, which are highlighted by the gray background. A sequence of arbitrary length is generated by repeating these four patterns to achieve the desired measurement count or duration. A configurable parameter of the sequence is the frequency f_1, which defines the frequency of the pattern. As a heterodyne approach is used later for phase unwrapping, the second frequency in the sequence is defined by $f_2 = f_1 - 1$. Using this sequence design, phase recovery is possible at any position k in the pattern stream g_k captured by the camera by evaluating three neighboring patterns. As a first step, the background component a is estimated according to Equation 3.

$$\mathrm{a}(x,y) \;=\; g_{k-1}(x,y) + g_{k+1}\,(x,y) \tag{3}$$

Next, the fringe patterns for both frequencies can be reconstructed by Equations 4 and 5, by removing the background component a and additionally diving by it to reduce the influence of reflectivity. Furthermore, the phase-shift ϕ_k (either 0 or π) of each pattern is applied. To avoid the amplification of noise for pixels which are not illuminated by the projector, for example due to shadowing, pixels in the signals which correspond to pixels in $g_k(x,y)$ below an intensity threshold are set to the corresponding values in $a(x,y)$.

$$s_1(x,y) \;= \frac{\frac{1}{2}\left(g_{k-1}(x,y) - g_{k+1}(x,y)\right)}{a(x,y)}\, e^{i\phi_{k-1}} \tag{4}$$

$$s_2(x,y) \;= \frac{\left(g_k(x,y) - a(x,y)\right)}{a(x,y)}\, e^{i\phi_k} \tag{5}$$

Subsequently, the local relative phase for each frequency is obtained by bandpass filtering to remove one of the mirrored spectra in both s_1 and s_2 in the frequency domain. By calculating the inverse Fourier transform of the filtered spectrum, an estimation of the analytic signal is obtained, allowing for the extraction of the local phase by calculating the argument of the complex signal. Phase unwrapping is performed by the heterodyne approach outlined in [12].

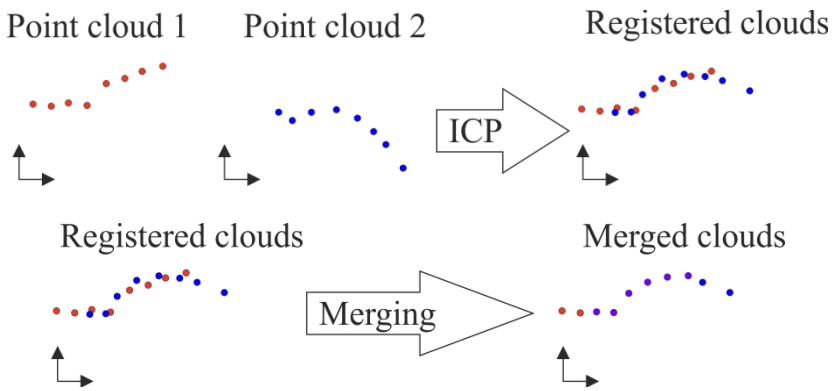

Figure 2: Illustration of registration process (top) and merging (bottom) of point clouds.

The proposed technique can also be used when projecting binary fringe patterns, as long as the bandpass filtering step is configured to suppress the higher fringe orders present for binary patterns.

4. REGISTRATION AND POSITION TRACKING

If measurements with relative motion between object and sensor head are performed, a registration step is required to combine multiple measurements in a common coordinate system. As a result, a complete dataset of the moving object is acquired, which can cover a much larger surface area than the individual datasets taken for example with the sequence proposed in Section 3. By performing registration, also the relative trajectory of the sensor head is estimated. The registration process is based on the trimmed ICP algorithm [13], which estimates a rigid transform to align two point clouds. The process is performed with each newly measured point cloud, leading to a growing number of points. In order to efficiently combine and store the high amount of point cloud measurements, which can be captured in short time using the interleaved sequence, a merging process is added after the registration of a new measurement. Points that lie within a certain Euclidian distance from each other in the two registered point clouds are merged to a point of weighted averaged position. The number of points which were merged to the average point position are stored and accumulated to the point's weight. This additionally enables the detection of outliers, by finding points which were only present in a single or few measurements of the sequence. Additionally, the logarithm of the point weights is used in the ICP algorithm to weight point correspondences in the registration procedure. It needs to be noted, that the registration and tracking is only unambiguous if the geometry exhibits distinctive features.

5. EXPERIMENTAL SETUP

The performance of different pattern sequences is evaluated on the basis of measurements acquired with a new fiber-endoscopic structured light sensor [2]. The measuring device consists of a pattern projector and industrial camera, which as coupled to high-resolution imaging fiber bundles with 100,000 individual cores each at a length of 1,000 mm. The distal ends of the fibers are fitted with gradient-index lenses to project pattern images onto a specimen's surface and capture the corresponding camera images via the detector fiber. Figure 3 left shows a close up photo of the sensor head with mirror prisms to achieve a sideways projection. The size of the measuring volume using this sensor head is approximately 8 mm in diameter and 4 mm in depth.

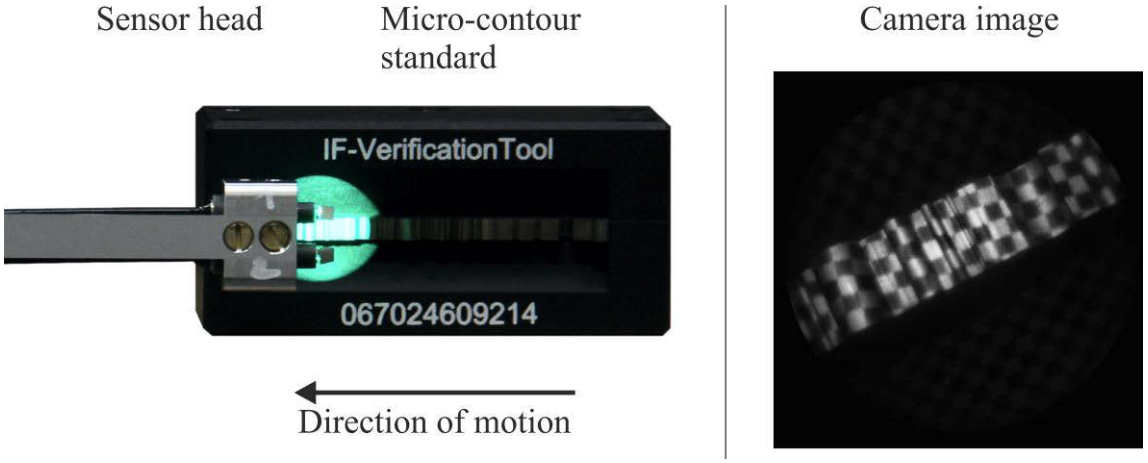

Figure 3: Endocopic Sensor head next to micro-contour standard (left). Corresponding camera image with checkerboard pattern illumination after CLAHE (right).

Evaluations are based on measurements of a micro-contour standard by Alicona, which features convex and concave cylindrical elements with calibrated radii, as shown in Figure 3 right. The metallic surface of the standard poses a challenged for structured light methods due to its varying reflectivity. Figure 3 right shows a camera image captured through the endoscope, which has been processed by contrast-limited adaptive histogram equalization (CLAHE) to reduce the dynamic range for viewing purposes.

For measurements in motion, the standard is mounted on a linear positioning stage and moved in the direction indicated in the figure. Three different pattern sequences with different parametrizations are compared, as shown in Table 1. To remove the influence of different total acquisition times to the measurements, the same pattern count is projected for all pattern sequences, by repeating the short sequence 2 times and projecting 10 patterns of the periodic interleaved sequence. This results in multiple measured phase maps for the shorter sequences, as shown in the last row. In order to reject noisy data points, values in the phase map with a local standard deviation in a 3x3 neighborhood of more than 0.1% the maximum range are masked out.

For the static case, multiple phase-maps for the short and interleaved pattern sequence are averaged to a single phase map for triangulation. For the measurements in motion, a point cloud is reconstructed independently from each phase map. In a second step, the measured point clouds for each sequence type are registered and merged using the technique described in Section 4. The distance threshold for merging neighboring points is defined to be 50 µm and the overlap parameter of the ICP algorithm set to 95%.

The maximum pattern rate achievable with the fiber-endoscopic sensor is limited by the camera (Point Grey GS3-U3-23S6M-C) of the system. The measurements using the linear stage are based on pattern captures at a resolution of 2.3 Mpixels at an intensity resolution of 12 bit. The pattern projection rate is set to the maximum of 132 Hz at exposure durations of 7.45 ms per pattern, resulting in a total acquisition time of 75.8 ms for all sequence configurations.

In addition to the measurements with motion by a linear positioning stage, a measurement of the complete contour of the standard is performed by moving the sensor head by hand. As higher velocities are expected in this case, the resolution of pattern captures is decreased by enabling the binning mode of the camera, resulting in a pattern rate of 180 Hz at exposure durations of approximately 5.5 ms. Additionally, the normalized frequency of the pattern has been reduced to 15 to increase the robustness of the phase-unwrapping process towards motion at the cost of a reduced lateral resolution

Table 1: Sequence configurations for the experiments.

Sequence type	Long	Short	Interleaved
Highest frequency normalized by image diameter	50	30	25
Phase shift count configuration for highest frequency	6	3	2
Additional pattern frequencies for unwrapping	2	1	1
Total pattern count for point cloud reconstruction	10	5	3
Measured point clouds after 10 projected patterns	1	2	8

6. RESULTS

The results for the measurements with the pattern configurations described in Section 5 are shown in Figure 4. Additional parameters of the measured point clouds are given in Table 2 and Table 3. For the non-moving scenario, the long pattern sequence is showing the lowest deviation to the calibrated radius of 1001.5 µm of the reference. In addition, the number of data points is higher than for the other sequences. The short and interleaved pattern sequences lead to less measured data points on the sides of the cylinder due to the lower amount of reflected light. Comparing the short sequence with the interleaved sequence shows a lower standard deviation for the radius feature. At the same time, the standard deviation of the distance of the individual data points to the fitted reference is lower, indicating higher noise in the data points measured with the interleaved pattern sequence.
When measuring the cylinder at a movement speed of 0.5 mm/s, the standard deviation of estimated cylinder radiuses is the lowest for the interleaved sequence, while the two conventional sequences show a similar standard deviation. However, the data sets of the short

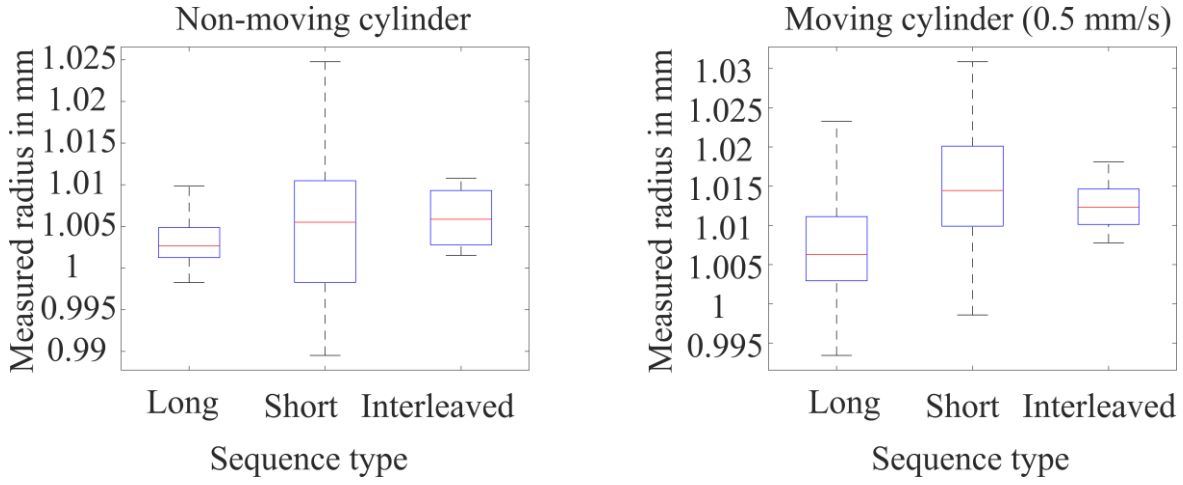

Figure 4: Measurement results for non-moving and moving cylindrical element.

Table 2: Parameters of measured point clouds for non-moving cylinder

Sequence type	Long	Short	Interleaved
Average point count	24486	18540	20876
Average standard deviation of points to reference	7.6 µm	8.7 µm	9.3 µm

Table 3: Parameters of measured point clouds for cylinder moving at 0.5 mm/s

Sequence type	Long	Short	Interleaved
Average point count	10555	17080	31298
Average standard deviation of points to reference	14.2 µm	12.9 µm	10.0 µm

and interleaved sequences, which were obtained by combining multiple measurements using the ICP approach outlined in Section 4, exhibit a mean deviation to the reference value of about 10 µm. The number of data points is decreasing with the length of the sequences, with the highest number for the interleaved sequence and the lowest for the long sequence. Contrary to the stationary measurement, here the point clouds feature less data points for the long sequence on the sides of the cylinder. Also, the standard deviation of measured data points compared to the fitted reference is the lowest for the interleaved sequence.
For the cylinder moving at 2.0 mm/s no valid data points could be measured for the long and short sequence. The results for the interleaved sequence for this movement speed are shown in Figure 5 on the left. Compared to the lower movement speed, the standard deviation of measured radii is increased. 35507 data points could be acquired on average on the surface, resulting in a dense point cloud.
Figure 5 right shows the results of a hand-guided measurement of the full geometry of the micro-contour standard. While the resolution of the measurement is decreased, all features of the micro-contour standard, consisting of concave and convex radius elements, steps, and angles are visible. Despite an increase in noise, features as small as the cylindrical feature

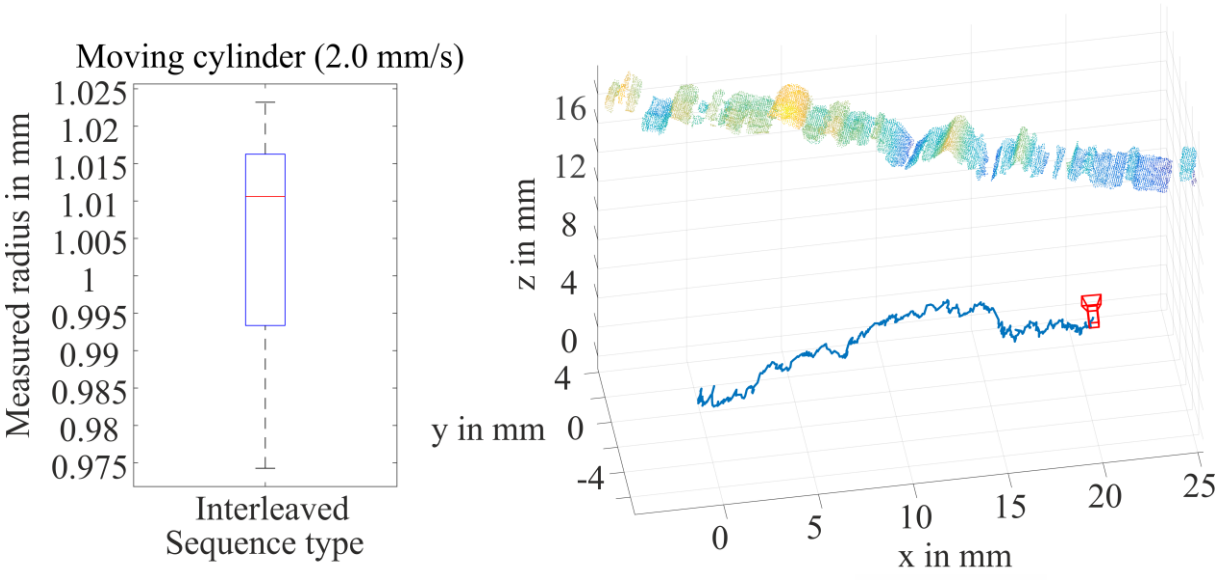

Figure 5: Measurement results for moving cylinder on linear positioning stage (right) and hand-guided measurement of the full contour-standard geometry (right).

with 100 µm radius are still discernible in the measurement. The path of the sensor head, estimated by using the registration and merging procedure outlined in Section 3, is shown in form of the blue line.

7. DISCUSSION

When measuring non-moving objects, best performance is achieved using a conventional pattern sequence with multiple phase-shifts and higher frequencies, as evident in the results in Table 2. Despite noise in the camera images owing to the very short exposure durations, 3-D point clouds can be measured with a point-reference standard deviation of less than 10 µm on the cylindrical element with a total acquisition time of less than 80 ms using the endoscopic sensor. For the non-moving cylinder, the pattern sequence introduced in Section 3 is performing better when compared with the shorter conventional sequence at the same acquisition time. This is a result of less measured points on the sides for the short sequence. The sides reflect less light towards the camera, leading to a lower signal-to-noise ratio for these areas.

Measurements in motion significantly benefit from the shorter acquisition time of individual measurements in the interleaved sequence. The number of acquired measuring points is significantly higher than for the longer sequence. Especially on the sides of the cylinder, fewer points are measured for the long sequence, leading to a less stable cylinder fit with higher standard variation when compared to the static measurements. The results for the interleaved sequence show a lower standard deviation of the measured radii when moving at 0.5 mm/s. Additionally, the point count is increased compared to the measurements without motion. This indicates that the registration and merging approach applied leads to improved results when compared to simple averaging of measured phase maps in the non-moving case. At a speed of 2 mm/s, no valid data points are captured using the conventional sequences. For the interleaved sequence, the number of data points is even higher than at lower speeds, as more data points can be measured on the sides of the cylinder resulting from variations in the perspective. However, the standard deviation of estimated radii is also increased, as a result from motion artifacts or the merging process.

A complete dataset of the contour standard could be acquired by moving the sensor head by hand. While individual measurements in the complete dataset suffer from motion artifacts and low point counts, the full dataset displays a dense reconstruction of the geometry. The combined result of a handheld measurement exhibits higher noise than the other measurements, however elements as small as 0.1 mm are still discernible. Motion artifacts are not evident in the dataset, as a result from the robust registration and merging procedure. Due to error propagation in the tracking of the sensor head, the full dataset appears slightly curved. Thus, the position estimation is growing more inaccurate with longer distances traveled.

In summary, the results show the feasibility of the proposed technique, which achieves dense point clouds even at velocities which equal 25% of the diameter of the measuring volume per second. The results could be achieved in the presence of the ambient illumination in the lab environment and a measuring object with varying reflectivity and specular highlights. Due to the relatively lower fringe frequencies employed and the bandpass filtering applied to separate the pattern components, the lateral resolution is lower when compared to the conventional sequences. In order to detect small geometry defects at the highest possible lateral resolution, relative motion between object and sensor head should be avoided. Additionally, ringing artifacts are experienced on objects with areas that are not illuminated by the pattern. These deviations could be reduced in the future by performing masking and symmetric interpolation for shadowed regions.

8. SUMMARY AND OUTLOOK

A pattern coding scheme for structured light measurements of dynamic scenes with highly varying reflectivity and non-continuous geometries has been proposed, which allows for fast 3-D rates. The sequence uses time-multiplexed phase-shift patterns in an interleaved projection scheme, which leads to high robustness towards an object's reflectivity and texture, while allowing a 3-D capture rate equally to the camera's image acquisition rate. At the same time, no constraints are imposed on the geometry of the measuring object or sensor setup. The feasibility of the method has been demonstrated by measurements of reference geometries as well as hand-guided measurements using a fiber-endoscopic structured light sensor. While the technique leads to a reduction of lateral resolution when compared to conventional pattern sequences, measurements are still possible at velocities equaling 25% of the diameter of the measuring volume per second. In combination with a robust registration and merging algorithm, hand-guided measurements of large geometries could be demonstrated using the endoscopic sensor.
In the future, the proposed technique could be used to track the position of the sensor head when performing inspection tasks in enclosed spaces. For this purpose, the sensor could be integrated into a continuum robot [14] for flexible positioning. The high measuring speed is also beneficial for measurements under the influence of vibrations, for example when inspecting industrial processes. By projecting binary interleaved patterns in combination with a high-speed camera, 3-D rates in the kHz range can be achieved.

ACKNOWLEDGMENT

The authors would like to thank the German Research Foundation (DFG) for funding the project B6 "Endoscopic geometry inspection" within the Collaborative Research Center (CRC) / TR 73.

REFERENCES

[1] Schwenke, Heinrich; Neuschaefer-Rube, Ulrich; Pfeifer, Tilo; Kunzmann, Horst (2002): Optical Methods for Dimensional Metrology in Production Engineering. In: CIRP Annals - Manufacturing Technology 51 (2), pp. 685–699.

[2] Matthias, Steffen; Loderer, Andreas; Koch, Sergej; Gröne, Michael; Kästner, Markus; Hübner, Sven et al. (2016): Metrological solutions for an adapted inspection of parts and tools of a sheet-bulk metal forming process. In Prod. Eng. Res. Devel. 10 (1), pp. 51–61.

[3] Salvi, Joaquim; Fernandez, Sergio; Pribanic, Tomislav; Llado, Xavier (2010): A state of the art in structured light patterns for surface profilometry. In: Pattern Recognition 43 (8), pp. 2666–2680.

[4] Gorthi, Sai Siva; Rastogi, Pramod (2010): Fringe projection techniques: whither we are? In Optics and lasers in engineering 48 (IMAC-REVIEW-2009-001), pp. 133–140.

[5] Lavoie, P.; Ionescu, D.; Petriu, E. (1999): A high precision 3D object reconstruction method using a color coded grid and NURBS. In : Proceedings / International Conference on Image Analysis and Processing. September 27 - 29, 1999, Venice, Italy, pp. 370–375.

[6] Zhang, Zhengyou (2012): Microsoft Kinect Sensor and Its Effect. In IEEE Multimedia 19 (2), pp. 4–10.

[7] Zuo, Chao; Huang, Lei; Zhang, Minliang; Chen, Qian; Asundi, Anand (2016): Temporal phase unwrapping algorithms for fringe projection profilometry. A comparative review. In Optics and lasers in engineering 85, pp. 84–103.
[8] Zhang, Z. H. (2012): Review of single-shot 3D shape measurement by phase calculation-based fringe projection techniques. In Optics and lasers in engineering 50 (8), pp. 1097–1106.
[9] Takeda, Mitsuo; Gu, Quan; Kinoshita, Masaya; Takai, Hideaki; Takahashi, Yosuke (1997): Frequency-multiplex Fourier-transform profilometry. A single-shot three-dimensional shape measurement of objects with large height discontinuities and/or surface isolations. In Appl. Opt. 36 (22), p. 5347.
[10] Weise, Thibaut; Leibe, Bastian; van Gool, Luc (2007): Fast 3D Scanning with Automatic Motion Compensation. In : IEEE Conference on Computer Vision and Pattern Recognition, 2007. CVPR'07 ; Minneapolis, pp. 1–8.
[11] Takeda, Mitsuo; Mutoh, Kazuhiro (1983): Fourier transform profilometry for the automatic measurement of 3-D object shapes. In: Appl. Opt. 22 (24), p. 3977.
[12] Towers, C. E.; Towers, D. P.; Jones, J.D.C. (2005): Absolute fringe order calculation using optimised multi-frequency selection in full-field profilometry. In Optics and lasers in engineering 43 (7), pp. 788–800.
[13] Chetverikov, D.; Svirko, D.; Stepanov, D.; Krsek, P. (2002): "The Trimmed Iterative Closest Point algorithm", Proceedings / 16th International Conference on Pattern Recognition, August 11 - 15, 2002, Québec City, QC, Canada, pp. 545–548, 2002.
[14] Amanov, Ernar; Granna, Josephine; Burgner-Kahrs, Jessica (2017): Toward improving path following motion: Hybrid continuum robot design. In : Robotics and Automation (ICRA), 2017 IEEE International Conference on. IEEE, pp. 4666–4672.

CONTACTS

Dipl.-Ing. S. Matthias steffen.matthias@imr.uni-hannover.de
Dr.-Ing. habil. M. Kästner markus.kaestner@imr.uni-hannover.de
Prof. Dr.-Ing. E. Reithmeier sekretariat@imr.uni-hannover.de